BeKm-1 Is a HERG-Specific Toxin that Shares the Structure with ChTx but the Mechanism of Action with ErgTx1

Mei Zhang,* Yuliya V. Korolkova,† Jie Liu,* Min Jiang,* Eugene V. Grishin,† and Gea-Ny Tseng*
*Department of Physiology, Virginia Commonwealth University, Richmond, Virginia, USA; and
†Shemyakin-Ovchinnikov Institute of Bioorganic Chemistry, Russian Academy of Sciences, Moscow, Russia

ABSTRACT Peptide toxins with disulfide-stabilized structures have been used as molecular calipers to probe the outer vestibule structure of K channels. We want to apply this approach to the human ether-a-go-go-related gene (HERG) channel, whose outer vestibule is unique in structure and function among voltage-gated K channels. Our focus here is BeKm-1, a HERG-specific peptide toxin that can suppress HERG in the low nM concentration range. Although BeKm-1 shares the three-dimensional scaffold with the well-studied charybdotoxin, the two use different mechanisms in suppressing currents through their target K channels. BeKm-1 binds near, but not inside, the HERG pore, and it is possible that BeKm-1-bound HERG channels can conduct currents although with markedly altered voltage-dependence and kinetics of gating. BeKm-1 and ErgTx1 differ in three-dimensional scaffold, but the two share mechanism of action and have overlapping binding sites on the HERG channel. For both, residues in the middle of the S5-P linker (the putative 583–597 helix) and residues at the pore entrance are critical for binding, although specific contact points vary between the two. Toxin foot printing using BeKm-1 and ErgTx1 will likely provide complementary information about the unique outer vestibule structure of the HERG channel.

INTRODUCTION

Human ether-a-go-go-related gene (*HERG*) encodes the pore-forming subunit of the rapid delayed rectifier K (I_{Kr}) channels (Sanguinetti et al., 1995; Trudeau et al., 1995). I_{Kr} plays a key role in maintaining the electrical stability of the heart (Tseng, 2001). Therefore inherited mutations in *HERG*, and more importantly adverse drug effects that suppress I_{Kr} function, are linked to congenital and acquired long QT syndrome (Roden and Balser, 1999). HERG is also expressed in noncardiac cell types (Rosati et al., 2000; Smith et al., 2002; Zhou et al., 1998; Faravelli et al., 1996), and may play significant roles under physiological (e.g., insulin secretion in pancreatic β-cells (Rosati et al., 2000)) or pathological conditions (e.g., cancer cell growth (Smith et al., 2002)). Therefore, agents that can suppress or enhance the HERG channel function may find important therapeutic applications other than antiarrhythmic therapy (Roche et al., 2002). From this point of view, it is essential to obtain structural information about domains in the HERG channel that are involved in determining drug binding affinity and specificity.

The HERG channel has a broad spectrum of drug sensitivity (Roden and Balser, 1999). Importantly, drug sensitivity of this channel seems to be tightly regulated by conformational changes around the outer mouth region during membrane depolarization (C-type inactivation (Smith et al., 1996)) (Wang et al., 1997; Numaguchi et al., 2000; Ulens and Tytgat, 2000; although see Chen et al., 2002). Therefore, information about the structure of HERG's outer vestibule and pore region and the nature of conformational changes underlying C-type inactivation is valuable. The outer vestibule of the HERG channel, as in other K channels, is lined mainly by loops linking the fifth transmembrane segment (S5) and the pore region, the S5-P linkers. HERG's S5-P linker is unique in that it is 2–3 times the length of S5-P linkers in other K channels (43 aa vs. 12–23 aa) (Liu et al., 2002). We have performed cysteine scanning mutagenesis experiments to probe the structural and functional role of this linker (residues 571–613) (Liu et al., 2002). The results suggest that the middle segment of this linker (residues 583–597) may form an amphipathic α-helix, and is involved not only in the pore function (C-type inactivation and K^+ selectivity) but also in the activation gating process. We proposed a model in which this α-helix is oriented parallel to the channel surface, capable of interacting with the pore entrance at one end and with the voltage-sensing domain at the other (Liu et al., 2002).

Our next step is to see whether these features can be built into a model of three-dimensional (3-D) structure. Crystal structures of K channels' pore-domains are available: KcsA crystal structure representing the pore in the closed state, and MthK crystal structure representing the pore in the open state (Doyle et al., 1998; Jiang et al., 2002). Homology modeling using these crystal structures as templates has been applied to several channels (Rauer et al., 2000; Capener et al., 2000; Lipkind and Fozzard, 1997). Unfortunately, this approach cannot be applied to the HERG channel for two reasons. First, the ''S5-P equivalent'' in the KcsA or MthK crystal does not have a well-defined structure (Doyle et al., 1998; Jiang et al., 2002). Second, the marked differences in the length and amino acid sequence in this region between HERG and KcsA or MthK make sequence alignment (a prerequisite for homology modeling) impossible (see Fig. 11 *A*).

Submitted November 14, 2002, and accepted for publication January 28, 2003.

Address reprint requests to Gea-Ny Tseng, PhD, Dept. of Physiology, Virginia Commonwealth University, 1101 E. Marshall St., Richmond, VA 23298. Tel.: 804-827-0811; Fax: 804-828-7382; E-mail: gtseng@hsc.vcu.edu.

0006-3495/03/05/3022/15 $2.00

Peptide toxins that can bind to the outer vestibule of the HERG channel will be useful tools to bring us closer to an understanding of the channel's structure. Known peptide toxins that modulate K channel function are usually short (30–40 aa), and contain three or four disulfide bonds (Tytgat et al., 1999). The reticulation of these disulfide bonds makes the peptide structures compact and rigid, amenable to structural analysis using NMR spectroscopy and suitable as ''molecular calipers'' to probe the structures of binding sites on their target channels (Miller, 1995). Indeed, peptide toxin ''foot printing'' using strategies such as mutant cycle analysis has been a useful way to deduce the spatial relationships of residues lining the outer vestibule of different K channels (Hidalgo and MacKinnon, 1995; Miller, 1995). Several HERG-specific peptide toxins are available: BeKm-1 (Korolkova et al., 2001), ErgToxin 1 (ErgTx1) (Gurrola et al., 1999), ErgTx2 (Lecchi et al., 2002), and CsEKerg1 (Nastainzyk et al., 2002). BeKm-1 belongs to the α-KTx subfamily, whereas the other three belong to the γ-KTx subfamily (Tytgat et al., 1999) (Fig. 1). Previously we have shown that ErgTx1 binds to the outer vestibule of the HERG channel (Pardo-Lopez et al., 2002). The binding site is probably formed by uncharged residues in the S5-P and P-S6 linkers of the HERG channel (Pardo-Lopez et al., 2002). The focus of this study is BeKm-1, whose NMR structure has been solved recently (Korolkova et al., 2002). Although BeKm-1 and charybdotoxin (ChTx) share the 3-D scaffold (Fig. 1 *A*), there are important differences between the two. ChTx binds to its target K channels (Maxi-K or Kv channels such as the *Shaker*) using the β_{II} surface (interaction surface), and the lysine residue at position 27 (K27) plays a critical role (Fig. 1 *A*) (Park and Miller, 1992; Goldstein and Miller, 1993; Ranganathan et al., 1996). In a ChTx/*Shaker* complex, the ε-amino group of K27 functions as a ''tethered'' K^+ ion. It protrudes into the pore, binding near the ''selectivity filter'' of the pore and occluding current flow. BeKm-1 has an arginine at the equivalent position (R27, Fig. 1 *A*). The guanidinium moiety of the arginine side chain is much bulkier than the amino group of a lysine, and cannot insert into the pore. This is why the K27R mutation of ChTx reduces its potency by >1000-fold (Goldstein et al., 1994). Therefore, BeKm-1 may bind to the HERG channel using a different domain. Indeed, a recent alanine mutagenesis study suggests that residues along the α-helix of BeKm-1 are critical for suppressing HERG (highlighted in Fig. 1 *A*) (Korolkova et al., 2002). There is a precedent: TsKapa (α-KTx 4.2) is selective for small-conductance, apamin-sensitive, Ca-activated K (SK) channels (Castle, 1999). Its interaction surface consists of the α-helix (K19) and the loop between β_I and the α-helix (R6 and R9) (Fig. 1 *A*) (Castle, 1999). It is conceivable that toxins using different domains as their interaction surface recognize receptors of different conformations, which in turn reflect differences in the structure of these K channels.

We have two main goals in this study: 1), to deduce the mechanism by which BeKm-1 suppresses the HERG current, and 2), to explore the BeKm-1 binding site on the HERG channel using the cysteine scanning mutagenesis approach. Our data show that BeKm-1 and ErgTx1 share important features in their interactions with the HERG channel, and the mechanism differs from the ''pore-plugging'' mechanism described for ChTx blockade of the *Shaker* channel. Furthermore, the two toxins' binding sites on the HERG channel overlap, but likely involve different contact points. Thus, BeKm-1 and ErgTx1 have different 3-D scaffold structures but may share similar functional topologies, whereas BeKm-1 and ChTx have similar scaffold structures but different functional topologies. These data implicate a unique outer vestibule structure of the HERG channel.

MATERIALS AND METHODS

Toxin preparation

The expression and purification of BeKm-1 was performed as described previously (Korolkova et al., 2001). Briefly, BeKm-1 was expressed in the periplasm of *Escherichia coli* (HB101) as a fusion protein with two IgG-binding domains (ZZ) of staphylococcal protein A. The HB101 cells were harvested and lysed by ultrasonication. After ultracentrifugation, BeKm-1 fusion protein in the supernatant was purified by an IgG-Sepharose 6FF column (Amersham Pharmacia Biotech, Piscataway, NJ). BeKm-1 was cleaved from the fusion protein by enterokinase. The recombinant toxin was purified from the cleavage mixture by chromatography on a reverse phase HPLC column (Delta Pak C_{18} 300-A pore, 3.9 × 300 mm, Waters, Milford, MA), followed by an ODS Ultrasphere column (4.6 × 150 mm, Beckman,

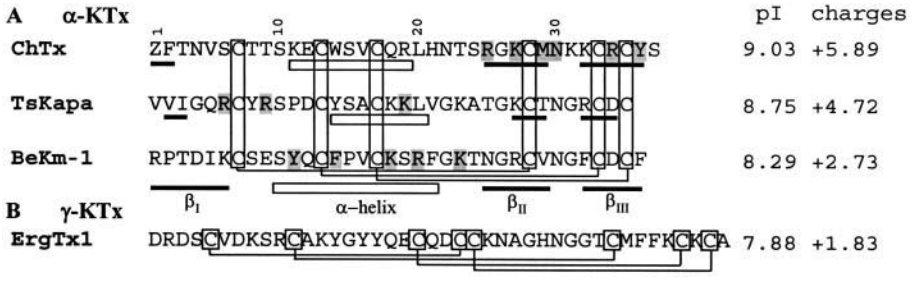

FIGURE 1 (*A*) Amino acid sequence alignment of BeKm-1 with two other members of the α-KTx family: charybdotoxin (ChTx) and TsKapa. Toxin position numbers are listed on top. Cysteine residues are boxed and connected based on the determined disulfide bridge pattern. Secondary structures are denoted: open horizontal bar (α-helix) and closed horizontal bars (β-strands, with β_I, β_{II}, and β_{III} marked below the BeKm-1 sequence). Toxin residues that have been shown to be critical for binding to target K channels are highlighted by gray shades. (*B*) The amino acid sequence and disulfide bridge pattern of ErgTx1, a member of the γ-KTx family. The isoelectric pH (pI) and net charges at pH 7 are shown to the right of each toxin sequence.

Fullerton, CA). Mass spectrometry verified the composition of the purified material. The toxin peptide content was determined using the bicincholinic acid method with bovine serum albumin (BSA) as the standard. Recombinant ChTx and ErgTx1 are obtained from Alomone (Jerusalem, Israel). The potency of the recombinant ErgTx1 in suppressing HERG (see Fig. 2) is very similar to that of native ErgTx1 previously determined under the same conditions (Pardo-Lopez et al., 2002). Lyophilized toxin powders were dissolved in 0.1% BSA in bath solution, aliquoted, and kept at −30°C. After thawing, each aliquot was kept on ice or at 4°C and used in <2 days.

Cysteine (Cys) scanning mutagenesis

Wild-type (WT) HERG in a vector, pAlterMax, was used to produce Cys mutants using the oligonucleotide-directed method and a commercial kit (Altered Site^R Mammalian Mutagenesis System, Promega, Madison, WI). Residues 571–613 (the S5-P linker), 631–638 (P-S6 linker), and 514–519 (S3-S4 linker) were substituted by Cys one at a time. In the following text, the mutants are designated by the WT residue (one letter code), followed by the position number and C for cysteine.

cRNA and oocyte preparations

cRNA was transcribed from cDNA using a commercial kit (T7 mMessage mMachine, Ambion, Dallas, TX), resuspended in DEPC-treated water, and the concentration was quantified by densitometry (ChemiImager Model 4000, Alpha Innotech, San Leandro, CA). Oocytes were isolated from *Xenopus laevis* and freed from follicular cell layers after mild collagenase treatment. Each oocyte was microinjected with 40 nl of cRNA solution (total cRNA 10–18 ng). After incubating the oocytes for 2–4 days at 16°C in an ND96 medium (composition given below) supplemented with horse serum (4%) and antibiotics (penicillin 50 U/ml and streptomycin 50 U/ml), channels were studied in electrophysiological experiments.

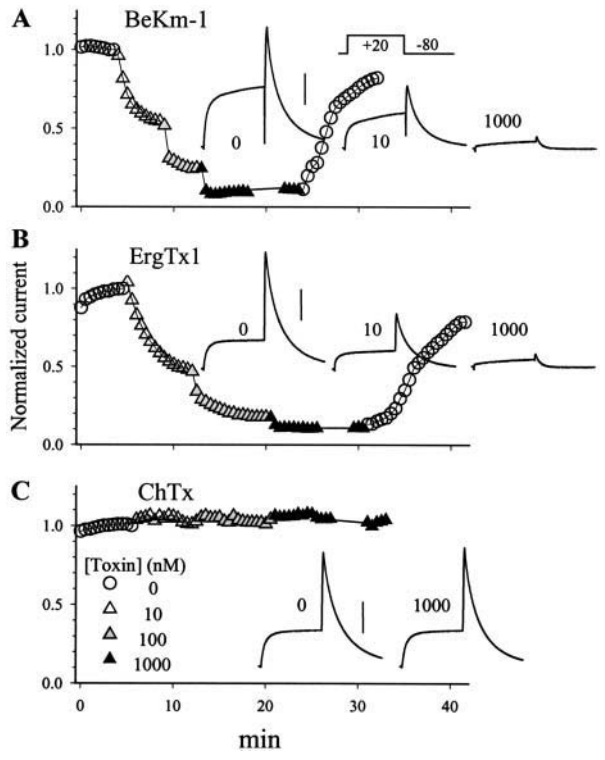

FIGURE 2 BeKm-1 and ErgTx1 both suppress HERG with a high potency, whereas ChTx has no effect at 100-fold higher concentration. Shown are time courses of changes in HERG current amplitude before, during, and after exposure to different concentrations of toxins (in nM, denoted by different symbols as shown in *panel C*). Currents are elicited by 1-s depolarization pulses from V_h −80 mV to +20 mV once every 30 s. The peak amplitudes of tail currents are measured and normalized by the control current amplitude right before toxin application. Inset of each panel depicts current traces recorded before (0) and during exposure to toxin at the concentration (in nM) marked, with leak currents subtracted. Calibration bars = 1 uA.

Electrophysiological experiments

Voltage clamp was done with the two-microelectrode method using an oocyte clamp amplifier (model 725B or 725C, Warner Instruments, Hamden, CT). Voltage clamp protocol generation and data acquisition were controlled by pClamp 5.5 via computer and a 12-bit D/A and A/D converter (Axon Instruments, Union City, CA). Unless otherwise stated, a typical experiment started with placing an oocyte in a tissue bath containing 0.8 ml of low-[Cl] bath solution (to avoid interference from endogenous Cl currents). The grounding electrodes were filled with 3 M KCl (in contact with Ag/AgCl pellets) and connected to the bath solution with salt bridges made of 1% agar in bath solution (to avoid perturbing ion composition in the small volume of static bath solution). The oocyte was impaled with two microelectrodes, and membrane currents were recorded. The membrane voltage was held at −80 mV (V_h), and currents were activated by a 1-s step to +20 mV applied once per 30 or 60 s. After control currents (I_C) were recorded, 5 ul of BeKm-1 stock solution (2 uM in 0.1% BSA) was diluted with 0.2 ml of bath solution and added to the bath (final [BeKm-1] 10 nM, unless otherwise stated). Repetitive pipetting was used to facilitate equilibration of toxin concentration in the bath. The remaining current in the presence of BeKm-1 (I_{TX}) was recorded when the degree of current suppression reached a steady state. For the determination of concentration-response relationship, the above procedure was modified. The beginning BeKm-1 concentration in the bath solution was 1 nM (from 0.2 uM stock) and was increased cumulatively after the steady-state effect was reached at each concentration (up to 100 nM). When higher concentrations of toxin were needed (experiments shown in Figs. 2, 6, 7, and 10), BeKm-1 stock solutions were made at 20 and 200 uM. ErgTx1 and ChTx were reconstituted and applied in the same manner. In some experiments (Fig. 3 *A*), oocytes were microinjected with salt solution immediately before recordings. This was done using the same device as for cRNA microinjection.

Solutions

The ND96 solution had the following composition (in mM): NaCl 96, KCl 2, $CaCl_2$ 1.8, $MgCl_2$ 1, HEPES 5, and Na-pyruvate 2.5. The solution was titrated to pH 7.5 with HCl. The standard low-[Cl] solution used during voltage clamp experiments had a similar composition, except that NaCl and KCl were replaced by NaOH and KOH, $MgCl_2$ was replaced by $MgSO_4$, and the pH 7.5 was adjusted to 7.5 with methanesulfonic acid. The following solutions were used in some experiments: a), 98 mM [K] solution, NaOH was replaced by equimolar KOH and Na-pyruvate was omitted; b), low ionic strength solution, NaOH was lowered to 20 mM using sucrose to maintain the osmolarity; c), different pH solutions, pH of the standard solution was titrated to 6.5 (with methanesulfonic acid) or 8.5 (with NaOH); and d), 50 mM TEA solution, the same as the standard low-[Cl] solution except that 50 mM Na was replaced by TEA.

Data analysis

Data analysis was performed using the following programs: Clampfit of pClamp 6 or 8 (Axon Instruments), Excel (Microsoft), PeakFit, and SigmaPlot (Jandel Scientific, San Rafael, CA). Pairwise statistical analysis was done using *t*-test (SigmaStat, Jandel Scientific). Multiple-group comparison was done using one-way ANOVA, followed by Dunn's test.

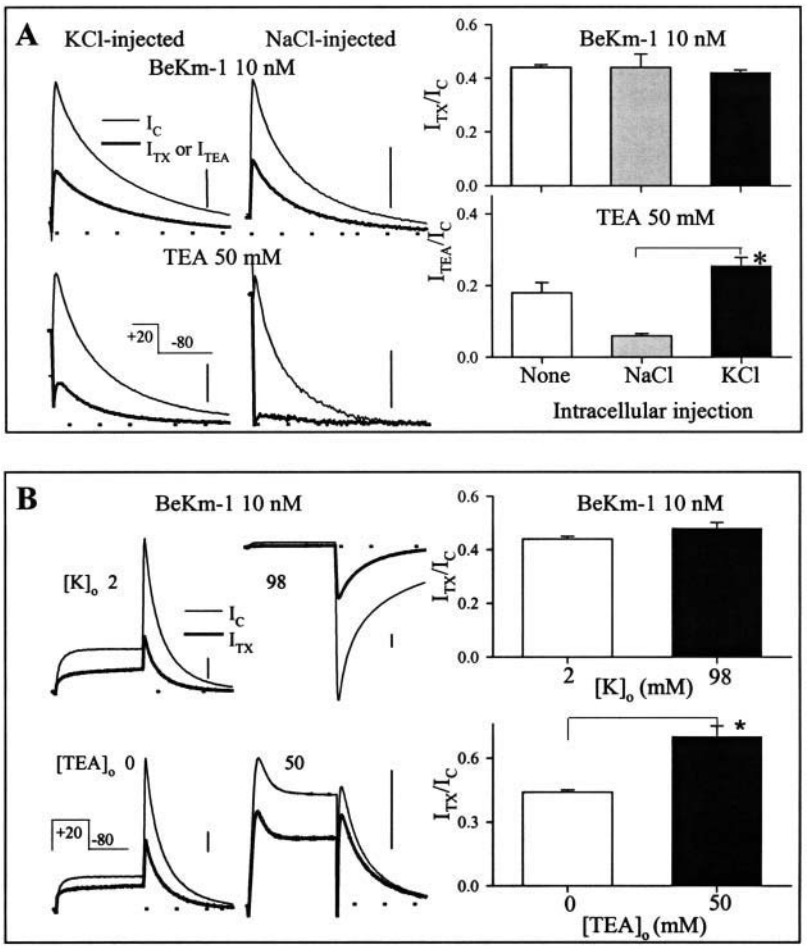

FIGURE 3 Effects of changing the intracellular or extracellular ionic composition on BeKm-1 suppression of HERG. (*A*) Increasing $[K]_i$ or $[Na]_i$ does not affect BeKm-1's potency but can influence the potency of a standard outer mouth blocker, TEA. Oocytes are injected with KCl or NaCl (see Methods, estimated increase in cytoplasmic salt concentration 50 mM), and tested for sensitivity to 10 nM BeKm-1 (*top*) or to 50 mM TEA (*bottom*). Left and middle panels, original tail current traces (elicited by the voltage clamp protocol shown in *lower left panel*) recorded from KCl-injected or NaCl-injected oocytes before (I_C) and after addition of BeKm-1 (I_{TX}) or TEA (I_{TEA}). Right panels, summary of ratios of tail currents in the presence of BeKm-1 or TEA to control from NaCl- or KCl-injected and uninjected oocytes ($n = 3 - 14$). (*B*) BeKm-1 potency is not affected by increasing $[K]_o$ from 2 to 98 mM (*top*), but is reduced by outer mouth occupancy by TEA (*bottom*). Left and middle panels, original current traces (elicited by the protocol shown in *lower left panel*) recorded in 2 and 98 mM $[K]_o$, or in the absence and presence of 50 mM TEA. Current traces before and after BeKm-1 (10 nM) application are denoted as in *A*. Right panels, summary of ratios of I_{TX} to I_C under specified conditions. Dotted lines are reference for measurement of peak tail current amplitudes. Calibration bars = 1 uA.

RESULTS

Fig. 2 compares the effects of BeKm-1, ErgTx1, and ChTx on HERG. Both BeKm-1 and ErgTx1 can suppress the HERG current in a concentration-dependent and reversible manner (Fig. 2, *A* and *B*). For both, the degree of suppression reaches around 50% at 10 nM. However, neither toxin can achieve a 100% suppression even at 1000 nM. Under these conditions, the current traces display the rectification property characteristic of the HERG channel (more outward current at −80 mV than at +20 mV), ruling out the possibility that these residual currents originate from oocyte endogenous or ''leak'' conductance. The basis for the residual HERG current seen in 1000 nM BeKm-1 will be discussed further in a later section.

In contrast to the high potency of BeKm-1 and ErgTx1, ChTx has no detectable effects on HERG at even 1000 nM (Fig. 2 *C*). Therefore, although BeKm-1 shares the 3-D scaffold with ChTx, its selectivity for HERG and the blocking potency are similar to those of ErgTx1 (Pardo-Lopez et al., 2002). However, a difference in the toxin potency does not necessarily reflect significant differences in the structure of the toxin binding site. For example, ChTx blocks the wild-type *Shaker* channel with a relatively weak potency (dissociation constant, K_d, 120 nM). A single point mutation, *Shaker*-F425G, can increase the potency of ChTx by 2000-fold (Stocker and Miller, 1994). A mechanistic study of toxin's actions should provide more insights into how the toxin binds to its receptor site and affect the channel function. To study the mechanism of BeKm-1 action, we characterize BeKm-1/HERG interaction in terms of its sensitivity to changes in the extracellular or intracellular ionic composition and to changes in membrane voltage. We compare these characteristics with those of ErgTx1/HERG and ChTx/*Shaker* interactions. The comparison with ChTx/*Shaker* is particularly informative because much has been learned about where ChTx binds to the *Shaker* channel and how it blocks the current (Park and Miller, 1992; Goldstein and Miller, 1993; Ranganathan et al., 1996; Gross and MacKinnon, 1996; Goldstein et al., 1994). This information can account for the well-defined features of ChTx/*Shaker* interaction: 1), The ChTx potency is reduced by an elevation of the intracellular or extracellular K^+ concentration ($[K]_i$ and $[K]_o$) (Ranganathan et al., 1996; Goldstein and Miller, 1993). This is because either intervention can increase K^+ ion occupancy inside the pore, which destabilizes binding of

the ε-amino group of K27 near the selectivity filter (Park and Miller, 1992). 2), The ChTx potency is reduced at stronger membrane depolarization (Goldstein and Miller, 1993). This occurs for two reasons. First, the increase in K^+ efflux through the pore at more depolarized voltages destabilizes binding of K27's ε-amino group. Second, membrane depolarization can also directly destabilize binding of this amino group because the binding site is ~20% down the transmembrane electrical field (Goldstein and Miller, 1993). And 3), The ChTx potency is enhanced by lowering the extracellular ionic strength (Goldstein and Miller, 1993; MacKinnon and Miller, 1989). This is because under these conditions the amplified attractive forces between positive charges on the toxin and negative charges on the outer vestibule of the channel can help direct/orient the toxin molecule toward its binding site (MacKinnon and Miller, 1989). Therefore, these aspects are where we begin to characterize BeKm-1/HERG interaction and to deduce the mechanism of toxin action.

Characteristics of BeKm-1/HERG interaction

Effects of increasing $[K]_i$ on BeKm-1/HERG interaction

BeKm-1 does not have a K27-equivalent (Fig. 1). However, mutating BeKm-1's K18, and to a lesser extent K23, to alanine can substantially reduce the toxin's potency (Korolkova et al., 2002), leaving it possible that BeKm-1 may block the HERG pore by a mechanism similar to that of ChTx using one of these lysine residues. In this case, we expect to see a reduction of BeKm-1 potency when $[K]_i$ or $[K]_o$ is elevated. Therefore, the first question is: is BeKm-1's potency reduced by increasing $[K]_i$? We use an approach similar to that described by Wang et al. (1996): oocytes are injected with concentrated NaCl or KCl solution (2.5 M, 10 nl per oocyte). The estimated increase in cytoplasmic salt concentration is 50 mM. Injected oocytes are immediately tested for BeKm-1 potency. To confirm that our approach can alter the cytoplasmic ion concentration and, more importantly, ion occupancy inside the HERG pore, we test the effects of NaCl or KCl injection on a standard outer mouth blocker, tetraethylammonium (TEA) (bottom panels of Fig. 3 *A*) (Smith et al., 1996). Compared with the TEA potency in suppressing the HERG current in uninjected oocytes, NaCl injection markedly accentuates the TEA potency, whereas KCl injection has a small (statistically insignificant) attenuating effect. The difference between NaCl-injection and KCl-injection is profound ($p < 0.001$). These data can be explained by proposing that a higher cytoplasmic Na^+ concentration can compete with K^+ ions for entry into the HERG inner mouth. This can decrease K^+ ion occupancy inside the pore. However, since Na^+ ions do not bind well to the selectivity filter or cannot reach as close to the outer mouth as K^+ ions, the stability of TEA binding to the outer mouth is increased after NaCl injection. On the other hand, although KCl injection can lead to a rise of $[K]_i$ by 50 mM, the overall impact on K^+ occupancy inside the pore is less because the oocyte has a normal cytoplasmic [K] around 120 mM. These data indicate that indeed we can perturb the cytoplasmic ion concentration and influence ion occupancy inside the HERG pore by intracellular injection of high [salt] solution. Top panels of Fig. 3 *A* show that compared to uninjected oocytes, neither NaCl nor KCl injection has any detectable effects on BeKm-1 potency. Therefore, unlike TEA, BeKm-1 binding to the HERG channel is not sensitive to changes in K^+ occupancy inside the pore.

Effects of increasing $[K]_o$ on BeKm-1/HERG interaction

Top panels of Fig. 3 *B* show that elevating $[K]_o$ from 2 to 98 mM has no effect on the BeKm-1 potency in suppressing HERG. This adds more support for the notion that BeKm-1 binding to the HERG channel is not affected by changing K^+ ion occupancy around the selectivity filter. This situation is different from that of ChTx/*Shaker* interaction (Ranganathan et al., 1996; Goldstein and Miller, 1993), but similar to that of ErgTx1/HERG interaction (Pardo-Lopez et al., 2002).

Effects of an outer mouth blocker, TEA, on BeKm-1/HERG interaction

Since BeKm-1 binding to the HERG channel is not sensitive to changes in either $[K]_i$ or $[K]_o$, our next question is: does BeKm-1 bind near the HERG outer mouth? One way to answer this question is to test whether the BeKm-1 potency is affected by an outer mouth blocker. For example, TEA can reduce the potency of both ChTx (in suppressing *Shaker* current) and ErgTx1 (in suppressing HERG) (Goldstein and Miller, 1993; Pardo-Lopez et al., 2002). The lower panels of Fig. 3 *B* show that the BeKm-1 potency is also significantly reduced when tested in the presence of 50 mM TEA. The sensitivity to TEA can be due to a steric effect (bound TEA hinders BeKm-1 access to its binding site), and/or a charge effect (the positive charge of bound TEA repels approaching positively charged BeKm-1 molecules). The latter effect occurs if positive charges on the BeKm-1 molecules can influence toxin binding. To test whether this is the case, we examine the effects of changing pH_o on BeKm-1 potency.

Effects of changing pH_o on BeKm-1/HERG interaction: difference between BeKm-1 and ErgTx1

BeKm-1 has a isoelectric pH (pI) of 8.29 and carries <3 positive charges at neutral pH_o (Fig. 1 *A*). Changing pH_o from 7.5 to 6.5 should increase the number of positive charges on the toxin molecule, whereas changing pH_o from 7.5 to 8.5 should abolish the positive charges or even make the toxin negatively charged. Fig. 4 *A* (*left panel*) shows that changing pH_o from 7.5 to 6.5 enhances BeKm-1 potency,

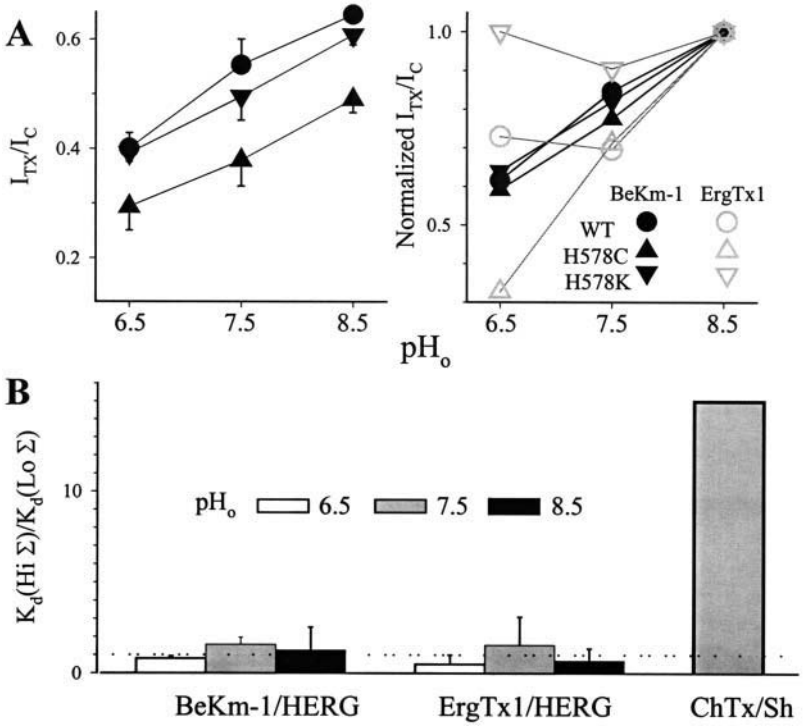

FIGURE 4 (*A*) Effects of changing pH_o on BeKm-1 suppression wild-type HERG (WT, *circles*) and two histidine mutants (H578C, *triangles*, and H578K, *inverted triangles*). Left, fractions of remaining current in the presence of 10 nM BeKm-1 (I_{TX}/I_C) measured at 3 pH_o levels. Voltage clamp protocol and current measurement are as described for Fig. 2. Right, comparison between BeKm-1 and ErgTx1 in the profile of pH_o sensitivity of toxin suppression of WT HERG and the two histidine mutants. The mean values of I_{TX}/I_C measured at pH_o 6.5 and 7.5 are normalized by the mean I_{TX}/I_C value at pH_o 8.5. BeKm-1 data are from the left panel using the same symbols. ErgTx1 data (*open gray symbols*) were obtained under the same conditions (Pardo-Lopez et al., 2002). (*B*) BeKm-1/HERG or ErgTx1/HERG interaction is insensitive to a decrease in extracellular ionic strength (Σ), in sharp contrast to ChTx/*Shaker* interaction. Degrees of current suppression by 10 nM BeKm-1 or ErgTx1 are measured in solution of normal ionic strength (high Σ, ND96 with 96 mM $[Na]_o$, Σ = 110 mM) and in solution of low ionic strength (low Σ, $[Na]_o$ reduced to 20 mM with sucrose substitution, Σ = 30 mM) at pH_o 6.5, 7.5, and 8.5. The I_{TX}/I_C values are used to estimate K_d values according to Eq. 1 (Fig. 7 legend, A_{max} = 0.9). The ratios of K_d in high Σ to that in low Σ are shown. To avoid interference from effects of H578 protonation on ErgTx1 potency, the effects of ErgTx1 are tested on H578C ((Pardo-Lopez et al., 2002), see *right panel* in *A*). The ChTx/Sh data is from MacKinnon and Miller (1989), where Σ is lowered from 110 to 50 mM.

whereas changing pH_o from 7.5 to 8.5 reduces BeKm-1 potency. These observations support the notion that BeKm-1 binding to the HERG channel is facilitated by positive charges on the toxin molecule.

This profile of pH_o sensitivity differs from that of ErgTx1 (Pardo-Lopez et al., 2002). The right panel of Fig. 4 *A* compares the profile of pH_o sensitivity between BeKm-1 and ErgTx1. To facilitate comparison, the fractions of remaining current in the presence of 10 nM toxin (I_{TX}/I_C) at pH_o 6.5 and 7.5 are normalized by that at pH_o 8.5. The degree of BeKm-1 suppression of HERG shows an almost linear profile in this pH_o range. On the other hand, although the potency of ErgTx1 (pI 7.88, Fig. 1 *B*) is increased as pH_o is acidified from 8.5 to 7.5 (indicating that positive charges on ErgTx1 can facilitate binding to HERG), the potency is not further increased at the pH_o 7.5–6.5 transition. Previously we have shown that this is due to a protonation of the histidine residue at position 578 (H578): the added positive charge can interfere with binding of positively charged ErgTx1 to the channel. Therefore, after replacing this histidine with cysteine (H578C), acidifying pH_o from 7.5 to 6.5 can cause a further increase in ErgTx1 potency. On the other hand, replacing the histidine with a ''permanent'' positive charge (H578K) markedly reduces the ErgTx1 potency at pH_o 6.5 and pH_o 7.5 (when the toxin is positively charged), but not at pH_o 8.5 (when the toxin is neutral or even negatively charged). On the other hand, neither H578C nor H578K affects the profile of pH_o sensitivity of BeKm-1/HERG interaction (although H578C modestly increases BeKm-1 potency, Fig. 4 *A*, *left panel*). Therefore, BeKm-1 differs from ErgTx1 in that binding of BeKm-1 to the HERG channel is shielded from the electrostatic repulsion of a positive charge at position 578.

Effects of lowering the extracellular ionic strength on toxin/channel interactions

We next test whether BeKm-1 binding to the HERG channel can be enhanced by lowering the external ionic strength. We run the test at pH_o 6.5, 7.5, and 8.5, because the number and sign of electrical charges on the toxin molecule, as well as around its binding site on the channel, can impact on the sensitivity of toxin-channel interaction to the surrounding ionic strength. Surprisingly, lowering the external ionic strength (from 110 to 30 mM) does not affect BeKm-1 binding at any of the 3 pH_o levels (Fig. 4 *B*). This is in sharp contrast to the high sensitivity of ChTx/*Shaker* interaction to a similar change in the external ionic strength (data from (MacKinnon and Miller, 1989) shown in Fig. 4 *B*) We also test how lowering the external ionic strength affects ErgTx1 suppression of H578C (to avoid the compounding effect of H578 protonation on ErgTx1 binding) at the 3 pH_o levels. Similar to BeKm-1, the ErgTx1 potency is unaltered by this intervention. Therefore, although positive charges on BeKm-1 and ErgTx1 facilitate toxin binding to the HERG channel, the electrostatic forces between toxin and the channel binding site are much weaker than those involved in ChTx/*Shaker* interaction. This can be partly due to differences

in the pI values, and thus the number of positive charges carried by these toxins at comparable pH_o (Fig. 1). Another important factor is differences in the binding site: negative charges on the outer vestibule of the *Shaker* channel are critical for ChTx binding (MacKinnon and Miller, 1989), whereas negative charges on the outer vestibule of the HERG channel are not important for ErgTx1 binding (Pardo-Lopez et al., 2002). This may also be the case for BeKm-1 (see below, Fig. 11 *A*).

Voltage-sensitivity of BeKm-1/HERG interaction

Similar to the voltage-sensitivity of ChTx/*Shaker* interaction (Goldstein and Miller, 1993), membrane depolarization in the range of 0–+60 mV can clearly, although modestly, reduce the BeKm-1 potency in suppressing HERG (Fig. 5). This cannot be due to an increase in K^+ efflux through the pore, because the prominent C-type inactivation process actually reduces K^+ efflux in this voltage range (indicated by the trace of normalized test pulse current, or I_t). The voltage sensitivity cannot be due to binding of a positively charged toxin moiety within the membrane electrical field that experiences electrostatic repulsion by the membrane depolarization, based on the above data showing that changing K^+ ion occupancy inside the pore does not perturb BeKm-1 binding. Further support is provided by the observations that although changing pH_o from 6.5 to 8.5 (that should abolish the positive charges on the toxin) reduces BeKm-1 potency, it does not abolish this voltage sensitivity (Fig. 5). We consider two possibilities. First, the voltage-sensitivity may result from voltage-dependent interactions between BeKm-1 and the binding site on the HERG channel. In this scenario, membrane depolarization decreases the BeKm-1 binding affinity, thus reducing the degree of current suppression. Second, this voltage-sensitivity may reflect the effects of BeKm-1 binding on HERG channel gating. In this scenario, toxin-bound HERG channels can still conduct currents. However, toxin binding alters channel gating by shifting the voltage-dependence of activation in the positive direction, so that current amplitude in the presence of BeKm-1 will increase as the voltage becomes more positive (and more toxin-bound channels become activated). The second possibility can explain the observation that BeKm-1 cannot totally suppress the HERG current even at 1000 nM, ~100-fold of the IC_{50} (Fig. 2 *A*).

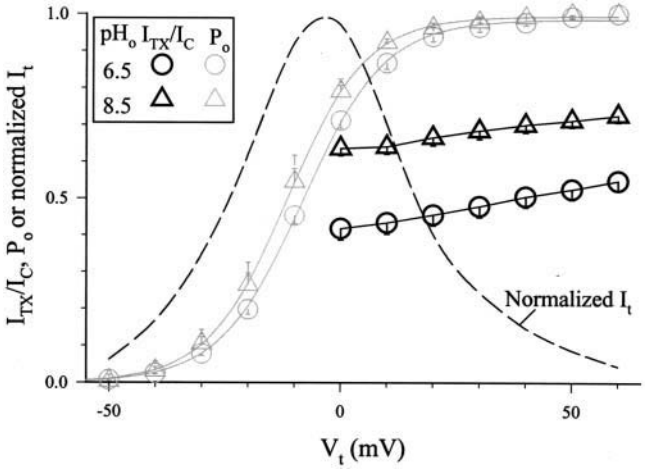

FIGURE 5 Voltage-sensitivity of BeKm-1 suppression of HERG and a comparison with voltage-dependence of channel activation and inward rectification. The following voltage clamp protocol is used: from V_h −80 mV, 1-s depolarization pulses to V_t −70 to +60 mV in 10 mV increments are applied once every 15 s. Peak tail current amplitudes (I_{tail}) are measured and the relationship between V_t and I_{tail} is fit with a single Boltzmann function to estimate the maximum tail current amplitude (I_{max}), half-maximum activation voltage ($V_{0.5}$), and slope factor (k): $I_{tail} = I_{max}/(1 + \exp((V_{0.5} - V_t)/k))$. I_{tail} amplitudes are normalized by estimated I_{max} (probability of opening, or P_o), averaged and plotted against V_t. This is done in pH_o 6.5 and 8.5, and shown as gray open symbols. The peak tail current amplitudes before (I_C) and after (I_{TX}) 10 nM BeKm-1 are measured and the I_{TX}/I_C values are plotted against V_t (*black open symbols*). The average test pulse current (I_t) of HERG at pH_o 7.5 normalized by the maximal I_t at 0 mV is shown as a dotted curve. Changing pH_o from 6.5 to 8.5 has little or no effects on the normalized I_t-V_t curve (Jiang et al., 1999).

Gating behavior of BeKm-1-bound HERG channels

To differentiate between these two possibilities, we analyze the voltage-dependence of HERG activation in the presence of 1000 nM BeKm-1 (when most channels are toxin-bound), and compare it to that seen at a much lower toxin concentration (10 nM, when both toxin-free and toxin-bound channels coexist). Fig. 6 *A* shows the HERG activation curve under the control conditions and in the presence of 1000 nM BeKm-1. With BeKm-1 on board, there is a prominent positive shift of the activation curve along the voltage axis ($V_{0.5}$ shifted from −17.4 ± 0.9 to +37.5 ± 3.2 mV), and a decrease in its slope (the k value increased from 9.0 ± 0.3 to 24.8 ± 1.7 mV). If this activation curve mainly reflects the gating behavior of toxin-bound/conducting HERG channels, then the activation curve in 10 nM BeKm-1 should have two widely separated components: one representing toxin-free channels and the other representing toxin-bound channels. Fig. 6 *B* shows such an analysis from six oocytes exposed to 10 nM BeKm-1. Under the control conditions, the activation curves follow a simple Boltzmann function. In the presence of 10 nM BeKm-1, the activation curves in all six oocytes require two Boltzmann components for a good fit. The negative component has parameter values indistinguishable from those of control activation curve, whereas the positive component has parameter values very similar to those of the activation curve seen in 1000 nM BeKm-1 (listed in Fig. 6 legend).

A further test of these two hypotheses is to analyze the HERG current kinetics in 1000 nM BeKm-1. Fig. 6 *C* shows the apparent HERG activation rates at +40 and +60 mV under the control conditions and in the presence of 1000 nM BeKm-1. With BeKm-1 on board, the time constant (τ) of

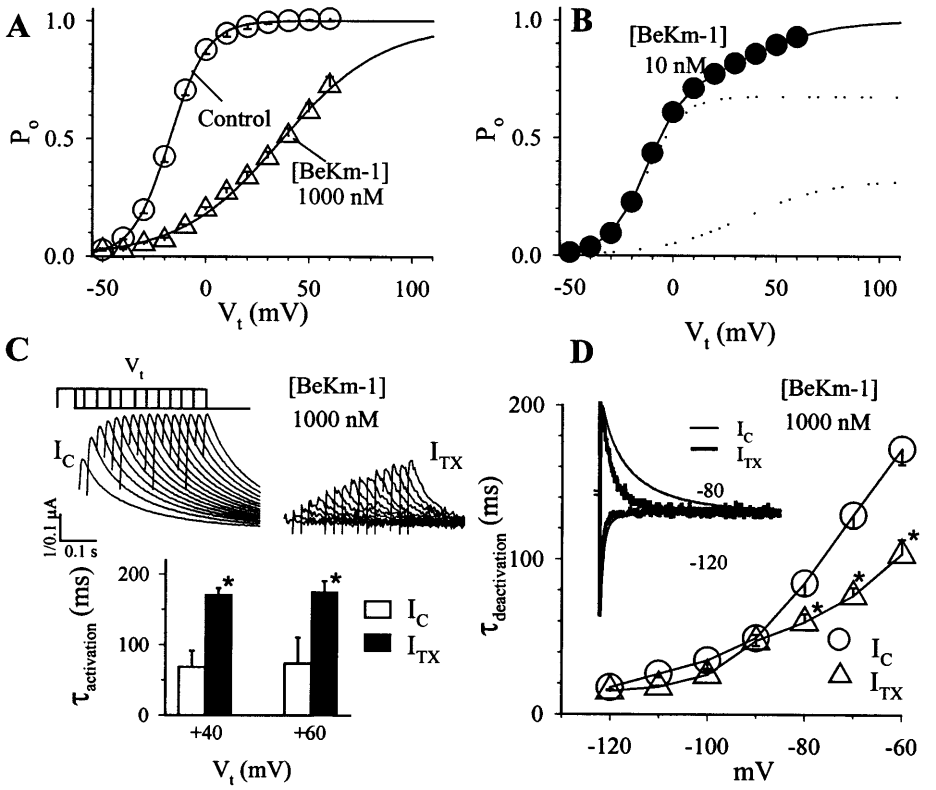

FIGURE 6 Effects of BeKm-1 on the activation gating properties of HERG. (*A*) Effects of 1000 nM BeKm-1 on the voltage-dependence of HERG activation. The voltage clamp protocol and current measurement/analysis are as described for Fig. 5. Control: $V_{0.5} = -17.4 \pm 0.9$ mV, $k = 9.0 \pm 0.3$ mV; in 1000 nM BeKm-1: $V_{0.5} = +37.5 \pm 3.2$ mV, $k = 24.8 \pm 1.7$ mV. (*B*) Activation curve in 10 nM BeKm-1. The voltage clamp protocol and current measurement are the same as those shown in *A*. The relationship between V_t and I_{tail} requires a double Boltzmann function for a good fit: $I_{tail} = I_1/(1 + \exp(V_1 - V_t)/k_1)) + I_2/(1 + \exp(V_2 - V_t)/k_2))$, where I_i, V_i, and k_i correspond to the I_{max}, $V_{0.5}$, and k of the ith Boltzmann component. The mean values are: $A_1 = 0.67 \pm 0.03$, $V_1 = -14.0 \pm 1.0$ mV, $k_1 = 8.0 \pm 0.3$ mV, $A_2 = 0.33 \pm 0.03$, $V_2 = +31.0 \pm 3.2$ mV, and $k_2 = 18.1 \pm 0.9$ mV. The dotted lines represent the two separate Boltzmann components. (*C*) Effects of 1000 nM BeKm-1 on time constant (τ) of activation determined by an envelope test. Top, voltage clamp protocol: membrane voltage is depolarized from V_h −80 mV to V_t for various durations and the degree of activation is tracked by the growth of peak amplitude of outward tail current following repolarization. Middle, superimposed tail current traces recorded before (I_C) and during (I_{TX}) BeKm-1 exposure with V_t to +40 mV. Envelope of peak tail current amplitudes is fit with a single exponential function to estimate $\tau_{activation}$. Bottom, summary of $\tau_{activation}$ at +40 and +60 mV. (*D*) Effects of 1000 nM BeKm-1 on τ of deactivation. Inset, superimposed tail currents recorded at −80 mV (*outward* or *upward*) and at −120 mV (*inward* or *downward*) before (*thin traces*) and during (*thick traces*) BeKm-1 exposure. The peak amplitudes of tail currents at the same V_r are matched to facilitate comparison. Data in panels *A*, *B*, *C* (*bottom*), and *D* (*main graph*) are averaged from 3–7 measurements each. *in *C* and *D*, $p < 0.05$.

activation is prolonged at both voltages (at +40 mV, from 68 ± 23 to 171 ± 9 ms). Fig. 6 *D* shows the apparent deactivation rates in the voltage range of from −60 to −120 mV under the control conditions and in the presence of 1000 nM BeKm-1. At voltages positive to −90 mV, the τ of deactivation is shortened by BeKm-1. The most marked change is at −60 mV: $\tau_{deactivation}$ is shortened from 171 ± 10 to 104 ± 10 ms. According to the first hypothesis, the slowing of HERG activation seen in BeKm-1 results from voltage-dependent toxin unbinding from the channel, whereas the acceleration of HERG deactivation reflects a voltage-dependent rebinding reaction. If this were the case, then these observed kinetic changes should be accounted for by published data of BeKm-1 unbinding and binding rate constants (Korolkova et al., 2002). The BeKm-1 unbinding rate constant is 0.02 s^{-1} (Korolkova et al., 2002). Therefore the time constant of BeKm-1 unbinding is 50 s, more than 200-fold longer than the observed time constant of HERG activation in 1000 nM BeKm-1. The BeKm-1 binding rate is 2.7×10^6 M^{-1} s^{-1} (Korolkova et al., 2002). At 1000 nM toxin concentration, the binding rate is 2.7 s^{-1}. This translates into a τ of binding reaction of 367 ms, much longer than the observed τ of channel deactivation seen in 1000 nM BeKm-1. Therefore, alterations in the kinetics of HERG activation and deactivation observed in the presence of 1000 nM BeKm-1 are much too fast to be accounted for by unbinding and rebinding reactions. Taken together, these observations support the notion that BeKm-1-bound HERG channels can conduct currents (although with reduced conductance), but have markedly altered gating kinetics.

The potency of ErgTx1 in suppressing HERG is also reduced by membrane depolarization (Pardo-Lopez et al., 2002). This voltage-sensitivity may be due to the same mechanism as is suggested by data shown in Fig. 2 *B*: in the presence of 1000 nM ErgTx1 the residual HERG current has markedly slowed activation and accelerated deactivation kinetics.

Apparent concentration-response relationship of BeKm-1 suppression of HERG

We examine the effects of 1–1000 nM BeKm-1 on the HERG current amplitude, using the same voltage clamp protocol and data analysis as those described for Fig. 2. The relationship between toxin concentration ([TX]) and fraction of remaining current (I_{TX}/I_C) are summarized in Fig. 7 (*open squares*, data obtained in 2 mM $[K]_o$, $n = 3$–14). Since I_{TX}/I_C results from a combination of toxin-free channels and

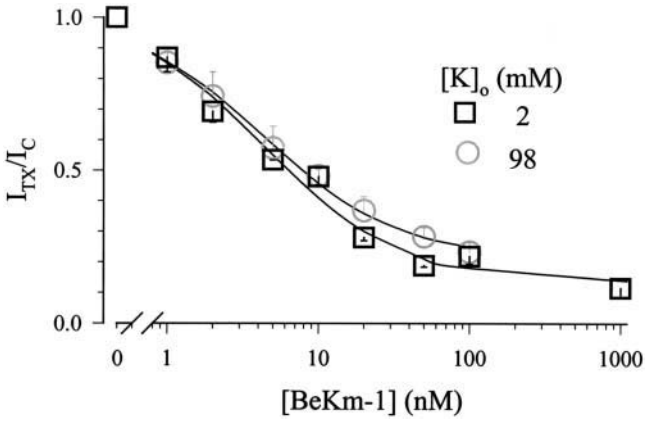

FIGURE 7 Concentration-response relationships of BeKm-1 suppression of HERG measured in 2 and 98 mM $[K]_o$. The voltage clamp protocol and current measurement are the same as those described for Fig. 2. Relationship between fraction of remaining current (I_{TX}/I_C) and toxin concentration ([TX]) is fit with the following equation: $I_{TX}/I_C = A_{max}/(1 + [TX]/K_d) + (1 - A_{max})$ (Eq. 1), where A_{max} is the fraction of toxin-sensitive current component and K_d is the dissociation constant. Each data point is summarized from 3 to 17 measurements. For 2 mM $[K]_o$, $A_{max} = 0.88 \pm 0.01$, and $K_d = 4.4 \pm 0.2$ nM. For 98 mM $[K]_o$, $A_{max} = 0.81 \pm 0.03$, and $K_d = 3.2 \pm 0.6$ nM (for both parameters, $p > 0.05$). The superimposed curves are calculated from Eq. 1, with the mean parameter values listed above.

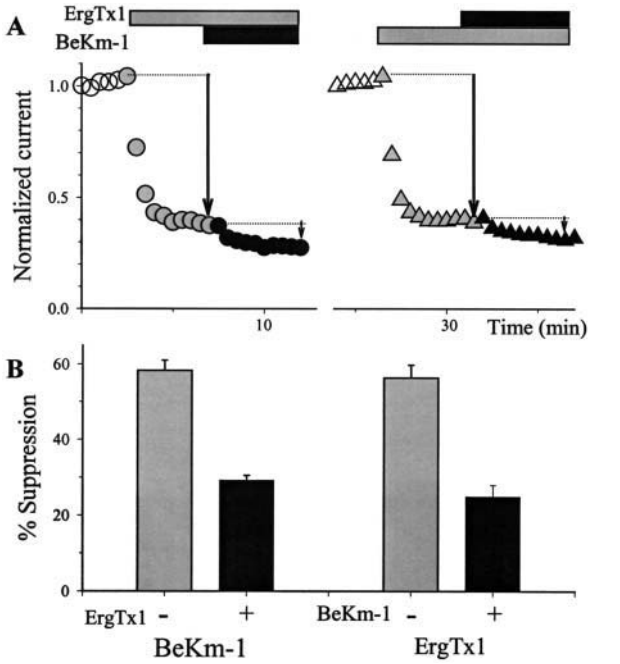

FIGURE 8 BeKm-1 application reduces the suppressing effects of subsequent ErgTx1 on HERG and vice versa. (*A*) Time course of changes in current amplitude from a representative experiment. The voltage clamp protocol and current measurement are the same as those described for Fig. 2. $[K]_o$ is 2 mM and [TX] for both BeKm-1 and ErgTx1 is 10 nM. The durations of toxin exposures are marked by horizontal bars on top. Toxin effects are washed out between 12 and 20 min. (*B*) Summary of BeKm-1 effects without or with preapplication of ErgTx1 (*left*) and ErgTx1 effects without or with preapplication of BeKm-1 (*right*). Data are pooled from six experiments. Three are done in the order shown in *A*, and the other three are done in the reverse order. The percentages of current suppression are calculated as illustrated by the arrows in *A*.

toxin-bound channels with altered conductance and gating kinetics, this concentration-response relationship does not reflect the molecular binding and unbinding events. Nevertheless, it serves as a quantitative description of toxin potency under the defined conditions. This apparent concentration-response relationship can be well described by the following equation:

$$I_{TX}/I_C = A_{max}/(1 + [TX]/K_d) + (1 - A_{max}), \qquad (1)$$

where A_{max} is the fraction of BeKm-1 sensitive current component (0.88 ± 0.01), and K_d is the apparent dissociation constant of BeKm-1 (4.4 ± 0.2 nM). Fig. 7 also shows that the potency of BeKm-1 is not affected by elevating $[K]_o$ from 2 to 98 mM, consistent with data presented in Fig. 3 *B*.

The concentration-response relationship of BeKm-1 is very similar to that of ErgTx1 (Pardo-Lopez et al., 2002). Both can be described by the same equation, with comparable K_d values and similar maximal effects (~90% suppression of the HERG current).

Finding the BeKm-1 binding site on the HERG channel

Is BeKm-1 binding site close to that of ErgTx1?

The above data indicate that BeKm-1 and ErgTx1 share similar features in their interaction with the HERG channel. Do they bind to the same or similar domains on the HERG channel? Fig. 8 *A* depicts the time course of a typical competition experiment. Application of ErgTx1 (10 nM) causes a 65% reduction in the HERG current. Subsequent application of BeKm-1 (10 nM) in the continuous presence of ErgTx1 causes only a 32% decrease in the current amplitude, measured relative to the current at the steady-state effect of ErgTx1. After washing out both toxins, the current amplitude recovers to near the control level. Toxins of the same concentration are applied in the reverse order. In this case, BeKm-1 alone causes a 60% decrease in the current amplitude whereas subsequent application of ErgTx1 causes only a 25% decrease. Fig. 8 *B* summarizes results from six experiments—three are done in the order shown in Fig. 8 *A*, and three are done in the reverse order. The effect of BeKm-1 is attenuated by a prior application of ErgTx1, and vice versa. This is consistent with the notion that the two toxins' binding sites on the channel may be close to each other.

Using the cysteine scanning mutagenesis approach to explore the BeKm-1 binding site

We examine the effects of cysteine mutations in the outer vestibule of HERG on BeKm-1 potency. The regions examined include positions 514–519 (S3-S4 linker), 571–613

(S5-P linker), and 631–638 (P-S6 linker) (Fig. 9 *A*). Recordings are made in 98 mM $[K]_o$ to enhance current amplitude of some poorly expressed mutants. This is justified because BeKm-1 binding to the HERG channel is insensitive to such a change in $[K]_o$ (Fig. 3 *B*). Currents are elicited by 1-s depolarization pulses to +20 mV, and peak amplitudes of tail currents at −80 mV are used to monitor the degrees of suppression by the toxin. Fig. 9 *B* depicts current traces of WT HERG and selected cysteine mutants in the absence and presence of 10 nM BeKm-1. The WT and N588C currents are markedly reduced by BeKm-1, whereas those of Q592C and P632C are not affected at all. For those cysteine mutants that show markedly reduced BeKm-1 sensitivity (W585C, G590C, Q592C, I593C, S631C, and P632C), toxin concentration is increased up to 200 nM when a discernible current suppression can be seen. The apparent K_d values are estimated by measurements based on one toxin concentration, using Eq. 1 with an assumed A_{max} value of 0.9 (Fig. 7). The K_d values are used to calculate mutation-induced changes in toxin binding free energy ($\Delta\Delta G$). Fig. 10 summarizes all the data: $\Delta\Delta G$ values are plotted against channel residues along the abscissa with selected position numbers labeled. The histogram bars are color coded by their $\Delta\Delta G$ values. Four cysteine mutations perturb toxin binding by >3 kcal/mol (*black histogram bars*, W585C, G590C, and Q592C in the 583–597 segment, and P632C in the P-S6 linker), two mutations perturb the binding energy in the 2–3 kcal/mol range (*gray histogram bars*, I593C in the 583–597 segment and S631C at the pore entrance), and six mutations perturb the binding energy in the 1–2 kcal/mol range (*hatched histogram bars*, I571C outside the S5, L589C, D591C, and P596C in the 583–597 segment, T613C at the pore entrance, and P605C). These data suggest the possibility that the BeKm-1 binding site on the HERG channel may be formed with contributions from the 583–597 segment of the S5-P linker and residues near the pore entrance (T613C and S631C).

However, cysteine substitution at a number of locations in the HERG's outer vestibule region can alter channel function. Specifically, these mutations can cause a disruption

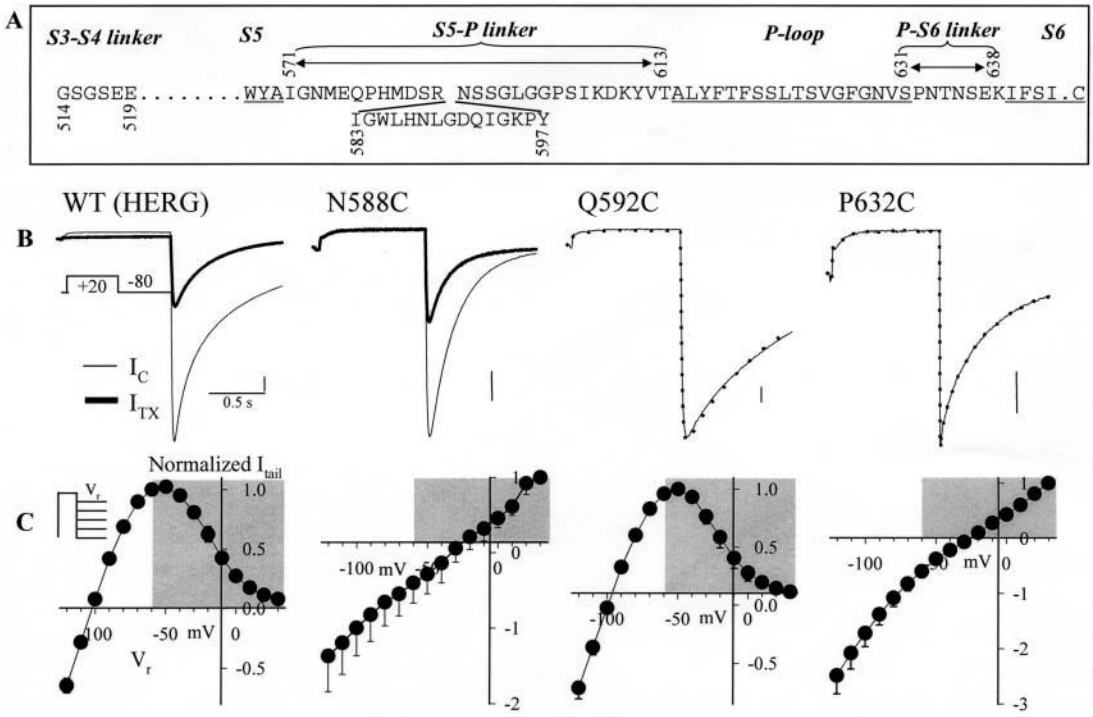

FIGURE 9 (*A*) Partial amino acid sequence of HERG in the outer vestibule region (from the end of S5 to the beginning of S6) and in the S3-S4 linker. Channel domains are marked on top. Position numbers of residues substituted by cysteine are noted: 514–519 of S3-S4 linker, 571–613 of S5-P linker (with 583–597 segment shown as an *insert*), and 631–638 of P-S6 linker. (*B*) Original current traces of WT and three selected cysteine-substituted mutants recorded before (I_C) and after (I_{TX}) application of 10 nM BeKm-1. Recordings are done in 98 mM $[K]_o$ using the voltage clamp protocol shown in inset of WT panel. (*C*) Current-voltage relationships of WT and the same three mutants. The voltage clamp protocol is diagrammed in the inset of WT panel: a 0.2 s conditioning pulse to +60 mV is used to activate (and inactivate) channels, followed by repolarization to V_r + 30 to −120 mV in 10 mV increments. Recordings are done in 2 mM $[K]_o$. The plateau or peak amplitudes of tail currents are measured, normalized by the maximal outward tail currents in the same oocyte (at −60 mV for WT and Q592C, and at +30 mV for N588C and P632C), averaged and plotted against V_r. The gray shades highlight the region of the I/V curves showing a negative slope in WT and Q592C (due to C-type inactivation) but a positive slope in N588C and P632C (due to a disruption of C-type inactivation). Note also the correlated difference in the reversal potential: ~−100 mV for WT and Q592, and ~−20 mV for N588C and P632C. Calibration bars = 1 uA.

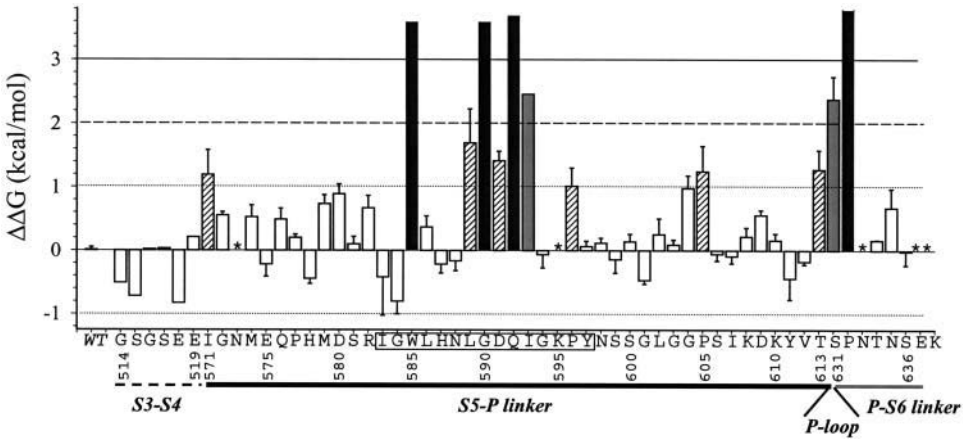

FIGURE 10 Effects of Cys substitutions in the S3-S4, S5-P, and P-S6 linkers of HERG on sensitivity to BeKm-1. The recording conditions, voltage clamp protocol, and current measurement are the same as those described for Fig. 9 *B*. One toxin concentration (10 nM) is used for WT HERG and all Cys mutants, except W585C, G590C, Q592C, I593C, S631C, and P632C. For these mutants that have markedly reduced BeKm-1 sensitivity, cumulative toxin concentrations of 50, 100, and 200 nM are used. The fraction of remaining current (I_{TX}/I_C) is used to estimate the K_d value according to Eq. 1 with $A_{max} = 0.9$ based on Fig. 7. The K_d value is used to calculate the mutation-induced alteration in binding free energy ($\Delta\Delta G$), according to: $\Delta\Delta G = RT\ln(K_d^{mut}/K_d^{WT})$, where K_d^{mut} and K_d^{WT} are the calculated K_d values for mutant and WT channels, and $RT = 0.6$ kcal/mol. The K_d^{WT} value averaged from these experiments in which one toxin concentration (10 nM) is used is 6.0 ± 0.4 nM ($n = 14$). For all the K_d^{mut} values, $n = 3 - 6$ each, but $n = 1$ for: 1), the six Cys mutants listed above where high BeKm-1 concentrations are used (although the lack of sensitivity to 10 nM BeKm-1 is confirmed in three or four measurements each), and 2), 514–519 mutants. Data are color coded based on the magnitudes of perturbation in binding free energy: white bars ($\Delta\Delta G < 1$ kcal/mol), hatched bars ($\Delta\Delta G$ between 1 and 2 kcal/mol), gray bars ($\Delta\Delta G$ between 2 and 3 kcal/mol), and black bars ($\Delta\Delta G > 3$ kcal/mol). Data are plotted against WT residues along the abscissa, with selected position numbers marked. The 583–597 segment is boxed. Channel domains S3-S4, S5-P, and P-S6 linkers are also marked. Oocytes expressing Cys mutants have been pretreated by DTT (5 mM, up to 4 h) and thoroughly rinsed in bath solution before recording. No data for the following mutants that have little or no expression: N573C, K595C, N633C, E637C, and K638C (marked by *).

of C-type inactivation, a decrease in the K^+ selectivity, and a negative shift in the voltage-dependence of activation (Liu et al., 2002). Two examples are illustrated in Fig. 9 *C*. The I-V curves of WT HERG and Q592C (a mutant with WT-like behavior) show a prominent negative slope in the voltage range from +30 to −60 mV. This is due to the strong C-type inactivation process that shuts down currents at positive voltages. Furthermore the reversal potential (E_{rev}) is very close to the predicted K^+ equilibrium potential (E_K), indicating a strong K^+ selectivity. On the other hand, the I-V curves of N588C and P632C show a positive slope in the same voltage range (C-type inactivation disrupted) and an E_{rev} around −10 mV (K^+ selectivity reduced). Therefore the interpretation of data presented in Fig. 10 can be compounded by the possibility that cysteine mutations may alter the BeKm-1 binding affinity by inducing global conformational changes in the outer vestibule that propagate to the toxin binding site. An argument against this possibility is shown in Fig. 9: cysteine substitution disrupts C-type inactivation and K^+ selectivity in N588C, but the BeKm-1 sensitivity is unaltered. On the other hand, Q592C has a WT-like behavior in terms of C-type inactivation and K^+ selectivity, but its BeKm-1 sensitivity is dramatically reduced. Such a dissociation between mutation-induced disruption of channel function and changes in BeKm-1 sensitivity is also clear from the summary data in Fig. 10. In addition to N588C, the following cysteine substituted channels have mutant (altered) channel behavior but the same BeKm-1 sensitivity as WT HERG: G572C, L586C, and T634C. Beside Q592C, the following channels have WT-like behavior but drastically reduced BeKm-1 sensitivity: P596C, T613C, and S631C.

Since BeKm-1's actions on the HERG channel have the characteristics of a ''gating modifier'' (depolarizing shift in the voltage-dependence of channel activation) (Swartz and MacKinnon, 1997a), we also examine the effects of cysteine substitution in the S3-S4 linker, a ''hot spot'' for binding of gating modifier toxins (Swartz and MacKinnon, 1997b; Li-Smerin and Swartz, 1998; Cestele et al., 1998). Cysteine substitutions in the S3-S4 linker do not affect BeKm-1 binding (Fig. 10).

DISCUSSION

Our findings can be summarized as the following: 1), BeKm-1 binds to the HERG channel near the pore entrance (because cysteine substitutions around the pore entrance or TEA binding to the pore reduce the toxin potency), without having a positively charged toxin moiety protruding into the pore (because toxin potency is insensitive to elevation in $[K]_i$ or $[K]_o$). 2), Positive charges on the toxin molecule facilitate binding to the channel (because acidifying pH_o from 8.5 to 6.5 increases positive charges on the toxin and enhances the toxin potency), but electrostatic forces are not a major factor in toxin/channel interaction (because the toxin potency is insensitive to lowering the external ionic strength, or to a neutralization of negative charges in the outer vestibule region: E575, D580, and D609). 3), BeKm-1-bound HERG channel can still conduct currents with a lowered conductance and drastically altered gating kinetics: more than +50 mV shift in the midpoint of activation curve, slowed activation, and accelerated deactivation. Therefore, BeKm-1 behaves both as a pore blocker and as a gating modifier. 4), Residues around the extracellular pore entrance and in the

583–597 segment of the S5-P linker are involved in forming the BeKm-1 binding site. And 5), S3-S4 linker is not involved in BeKm-1 binding.

Unique outer vestibule structure of the HERG channel

We have proposed that the outer vestibule of the HERG channel is unique among K channels. This is indicated by a comparison of amino acid sequences between HERG and other K channels: the S5-P linker that lines the outer vestibule of K channels is much longer in HERG (43 aa) than in other K channels (12–23 aa) (e.g., Fig. 11 *A*). This uniqueness is also indicated by the functional aspects of the HERG channel. The C-type inactivation process, which reflects conformational changes around a channel's outer mouth, is much faster and voltage-sensitive in HERG than in other Kv channels (Spector et al., 1996). The uniqueness is further supported by the cysteine mutagenesis data (Liu et al., 2002): mutations introduced into the middle of the S5-P linker, not contiguous with the channel pore in one-dimensional sequence, can have profound effects on the HERG's pore properties (C-type inactivation and K:Na selectivity) and the voltage-dependence of activation. We have proposed that positions 583–597 in the HERG's S5-P linker form an amphipathic α-helix, with its amino end near the channel pore and carboxyl end close to the voltage-sensing domain. In this model, the 583–597 helix serves as a bridge of communication between the pore and the voltage-sensing domain. Our findings here are consistent with such a topology: the 583–597 segment and the pore entrance are close to each other in 3-D space so that residues in these two regions together form the BeKm-1 binding site.

Although BeKm-1 shares the 3-D scaffold with other α-KTx members, its mechanism of action and interaction surface differ from those of ChTx and AgTx2 (Fig. 11 *B*).

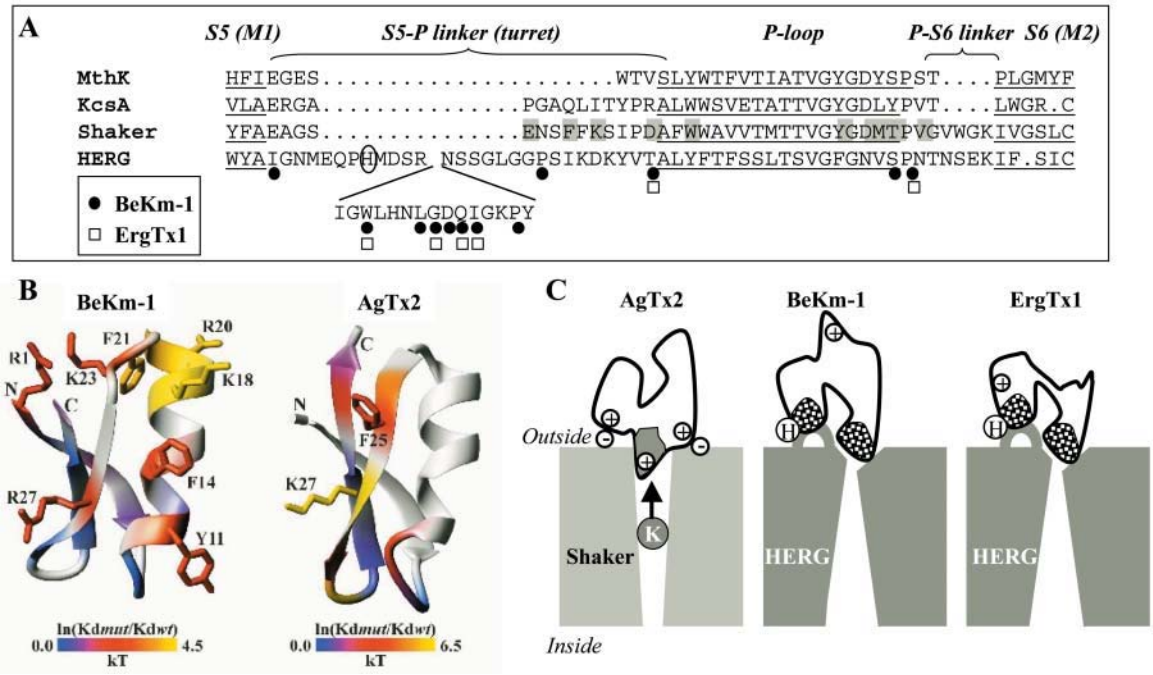

FIGURE 11 (*A*) Alignment of partial amino acid sequences of MthK, KcsA, *Shaker*, and HERG. S5 (equivalent to M1 in MthK and KcsA), P-loop, and S6 (M2) are underlined. S5-P linker (equivalent to ''turret'' in KcsA) and P-S6 linkers are delineated on top. Gaps (denoted by *periods*) are introduced to improve the alignment. For HERG, the segment from positions 583 to 597 is shown as an insert. Gray shades highlight the *Shaker* residues important for ChTx or AgTx2 binding. HERG residues important for BeKm-1 and ErgTx1 binding ($\Delta\Delta G > 1$ kcal/mol, Fig. 10 and Pardo-Lopez et al. (2002)) are highlighted by solid circles and open squares, respectively. H578 is circled. (*B*) NMR structures of BeKm-1 and AgTx2, color coded by the effects of mutations on binding affinity for HERG and *Shaker*, respectively. (*C*) Cartoon highlighting the differences and similarities in toxin-channel interactions: AgTx2 binding to the *Shaker* channel and BeKm-1 or ErgTx1 binding to the HERG channel. AgTx2 and BeKm-1 are shown as having the same 3-D scaffold (denoted by the same 2-D contour), but differ in: a), interaction surface used to bind to the outer vestibule of their target K channels, b), amount of net positive charges on the toxin surface, c), electrostatic forces involved in toxin-channel interaction, and d), ability to experience repulsion by K^+ ions inside the pore. The *Shaker* and HERG channels are each depicted as a solid structure with a central channel pore, but differ in: a), the outer mouth dimension (wider in *Shaker* than in HERG), b), inner mouth dimension (wider in HERG than in *Shaker*), and c), an α-helix formed by the 583–597 segment of S5-P linker in the HERG outer vestibule (depicted as a *semicircle*). ErgTx1 is depicted as having a very different 3-D structure (denoted by a 2-D contour different from those of AgTx2 or BeKm-1), but using an interaction surface similar to that of BeKm-1. BeKm-1 and ErgTx1 differ in their response to protonation of a histidine residue (H578) in the 583–597 α-helix of the HERG channel (*H* attached to the *semicircle*).

These points are symbolized in Fig. 11 *C*. In the cartoon, the HERG outer mouth is narrower than that of the *Shaker* channel. There are two reasons for this assumption. First, several hydrogen bonds that are important in maintaining the *Shaker* outer mouth in the open configuration (Larsson and Elinder, 2000) are missing in the HERG channel (Doyle et al., 1998). This will make the HERG outer mouth more flexible and easier to collapse. Second, the flexibility of HERG's outer mouth may allow part of the S5-P linker, e.g., the 583–597 α-helix, to line the pore entrance. This will narrow the outer mouth diameter. The cartoon in Fig. 11 *C* also shows a wider inner cavity in the HERG channel than that of the *Shaker* channel. This is in keeping with the observations that many chemicals can enter the inner mouth of the HERG channel and become trapped inside the pore by the closure of the cytoplasmic activation gate (Mitcheson et al., 2000).

BeKm-1 and ErgTx1 are useful tools to probe the structure of the outer vestibule of the HERG channel

BeKm-1 and ErgTx1 differ in their disulfide bridging pattern and do not share any significant homology in the amino acid sequence (Fig. 1). In terms of interaction with the HERG channel, BeKm-1 and ErgTx1 share the following features: 1), concentration-response relationship (apparent 1:1 binding stoichiometry with a maximum of ~90% suppression of current amplitude); 2), sensitivity to pH_o (acidifying pH_o enhances toxin-HERG interaction); 3), sensitivity to TEA (50 mM TEA significantly attenuates toxin potency); 4), insensitivity to elevating $[K]_o$ (from 2 to 98 mM); 5), insensitivity to lowering the external ionic strength (from 110 to 30 mM); and 6), voltage-sensitivity (depolarization modestly reduces the apparent potency of both toxins). The voltage-sensitivity of these two toxins may arise from the same mechanism: toxin-bound channels conduct currents but with altered gating kinetics. Furthermore, the two toxins attenuate each other's potency in suppressing the HERG current, suggesting that their binding sites on the HERG channel are close to each other or overlap.

We propose that BeKm-1 and ErgTx1 suppress the HERG current by the same mechanism, and share similarities in their interaction surfaces (Fig. 11 *C*). However, there are also important differences between BeKm-1 and ErgTx1 in terms of their contact points with the channel and the binding site environment. First, the impact of protonating histidine at position 578 at acidic pH_o on toxin binding differs between BeKm-1 (no impact) and ErgTx1 (reduced binding). Second, cysteine substitutions at the following positions affect BeKm-1 binding, but not ErgTx1 binding: I571, L589, D591, P596, P605, and S631 (Fig. 11 *A*). In particular, the difference in the impact of S631C (a mutation right at the edge of the pore entrance) suggests that BeKm-1 may bind deeper into the pore than ErgTx1, and thus senses the effects of mutating the 631 side chain. Mutant cycle analysis with BeKm-1 and ErgTx1, the latter's NMR structure, is available (Torres et al., 2003) and provides important insights into the unique structure of the outer vestibule of the HERG channel.

BeKm-1 as a gating modifier?

Although BeKm-1 binding has profound effects on the activation gating process of the HERG channel, its binding site and mechanism of action differ from those of hanatoxin, a well studied K channel gating modifier toxin (Swartz and MacKinnon, 1997b; Li-Smerin and Swartz, 2000). Hanatoxin binds to the S3-S4 linker of DRK1 with a 4:1 stoichiometry, and mutations in the pore and outer vestibule region have no effects on toxin binding. On the other hand, cysteine substitutions in HERG's outer vestibule region, but not in the S3-S4 linker, have marked effects on BeKm-1 binding, and the apparent concentration-response relationship can be described by a 1:1 stoichiometry. Therefore, BeKm-1 does not act like a ''conventional'' gating modifier (Li-Smerin and Swartz, 1998). We propose that the effects of BeKm-1 on HERG gating are due to the unique role of S5-P linker in this channel: S5-P linker is critically involved in the gating transitions that lead to the opening of the HERG pore (Liu et al., 2002). Therefore, a bound BeKm-1 molecule that makes contacts with this linker can have marked impact on the voltage-dependence and kinetics of activation and deactivation.

Technical consideration

In this study, we test the BeKm-1 potency on HERG channels expressed in *Xenopus* oocytes using a static bath volume of 1 ml. There are two concerns in this experimental design. First, the oocyte cell membrane has invaginations that may hinder the access of peptide toxin to a subpopulation of channels deep in the invaginations. Can this account for the BeKm-1-insensitive component of HERG current as shown in Fig. 2 *A*? If indeed there were a subpopulation of HERG channels inaccessible to the peptide toxin, a corollary is that the markedly altered gating behavior seen in the presence of 1000 nM BeKm-1 should largely reflect the gating properties of these inaccessible HERG channels (Fig. 6 *A*). Under the control conditions, no such current component is ever seen. Therefore, we conclude that the current component seen in the presence of 1000 nM BeKm-1 mainly represents the residual current through toxin-bound channels. Second, can there be a problem of toxin depletion in the static bath? The problem of peptide sticking to the plastic tissue well can be reduced by including 0.1% bovine serum albumin in the solution (see Materials and Methods). However, at low concentrations the toxin may still be partially depleted due to nonspecific binding to the oocyte cell surface. Although we cannot be certain as to the degree of toxin depletion in our experiments, it is important to point

out that the BeKm-1 potency estimated in our experiments (apparent K_d of 4.4 nM, with a maximal effect of 88% reduction) is not very different from that estimated by testing the toxin potency on HERG expressed in HEK 293 cells using a flowing bath (K_d 3.3 nM, with ~90% reduction at 100 nM) (Korolkova et al., 2001). It is also important to point out that using a static bath does not allow us to measure the rate constants of toxin binding and unbinding, which are essential in gaining mechanistic information about toxin-channel interactions.

The authors thank Dr. L. D. Possani for providing the native ErgTx1 for part of the experiments shown in Fig. 4 *B*, and Dr. Eduard V. Bocharov for helping preparing Fig. 11 *B*.

This study is supported by grants HL 46451 and HL 67840 from the National Heart, Lung and Blood Institute, National Institutes of Health, and a grant-in-aid from the American Heart Association Mid-Atlantic Affiliate, to G.-N.T., and grant 01-04-48338 from the Russian Foundation of Basic Research to E.V.G.

REFERENCES

Capener, C., I. Shrivastava, K. Ranatunga, L. Forrest, G. Smith, and M. Sansom. 2000. Homology modeling and molecular dynamics simulation studies of an inward rectifier potassium channel. *Biophys. J.* 78:2929–2942.

Castle, N. 1999. Recent advances in the biology of small conductance calcium-activated potassium channels. *In* Perspectives in Drug Discovery and Design 15/16. H. Darbon and J. Sabatier, editors. Kluwer, The Netherlands. 131–154.

Cestele, S., Y. Qu, J. Rogers, H. Rochat, T. Scheuer, and W. Catterall. 1998. Voltage sensor-trapping: enhanced activation of sodium channels by β-scorpion toxin bound to the S3-S4 loop in domain II. *Neuron.* 21:919–931.

Chen, J., G. Seebohm, and M. Sanguinetti. 2002. Position of aromatic residues in the S6 domain, not inactivation, dictates cispride sensitivity of HERG and eag potassium channels. *Proc. Natl. Acad. Sci. USA.* 99:12461–12466.

Doyle, D., J. Cabral, R. Pfuetzner, A. Kuo, J. Gulbis, S. Cohen, B. Chait, and R. MacKinnon. 1998. The structure of the potassium channel: molecular basis of K^+ conduction and selectivity. *Science.* 280:69–77.

Faravelli, L., A. Arcangeli, M. Olivotto, and E. Wanke. 1996. A HERG-like K^+ channel in rat F-11 DRG cell line: pharmacological identification and biophysical characterization. *J. Physiol.* 496:13–23.

Goldstein, S., and C. Miller. 1993. Mechanism of charybdotoxin block of a voltage-gated K^+ channel. *Biophys. J.* 65:1613–1619.

Goldstein, S., D. Pheasant, and C. Miller. 1994. The charybdotoxin receptor of a *Shaker* K^+ channel: peptide and channel residues mediating molecular recognition. *Neuron.* 12:1377–1388.

Gross, A., and R. MacKinnon. 1996. Agitoxin footprinting the *Shaker* potassium channel pore. *Neuron.* 16:399–406.

Gurrola, G., B. Rosati, M. Rocchetti, G. Pimienta, A. Zaza, A. Arcangeli, M. Olivotto, L. Possani, and E. Wanke. 1999. A toxin to nervous, cardiac, and endocrine ERG K^+ channels isolated from *Centruroides noxius* scorpion venom. *FASEB J.* 13:953–962.

Hidalgo, P., and R. MacKinnon. 1995. Revealing the architecture of a K^+ channel pore through mutant cycles with a peptide inhibitor. *Science.* 268:307–310.

Jiang, M., W. Dun, and G.-N. Tseng. 1999. Mechanism for the effects of extracellular acidification on HERG channel function. *Am. J. Physiol.* 277:H1283–H1292.

Jiang, Y., A. Lee, J. Chen, M. Cadene, B. Chait, and R. MacKinnon. 2002. The open pore conformation of potassium channels. *Nature.* 417:523–526.

Korolkova, Y., E. Bocharov, K. Angelo, I. Maslennikov, O. Grinenko, A. Lipkin, E. Nosireva, K. Pluzhnikov, S.-P. Olesen, A. Arseniev, and E. Grishin. 2002. New binding site on the old molecular scaffold provides selectivity of HERG-specific scorpion toxin BeKm-1. *J. Biol. Chem.* 277:43104–43109.

Korolkova, Y., S. Kozlov, A. Lipkin, K. Pluzhnikov, J. Hadley, A. Filippov, D. Brown, K. Angelo, D. Strobaek, T. Jespersen, S.-P. Olesen, B. Jensen, and E. Grishin. 2001. An ERG channel inhibitor from the scorpion *Buthus eupeus*. *J. Biol. Chem.* 276:9868–9876.

Larsson, H., and F. Elinder. 2000. A conserved glutamate is important for slow inactivation in K^+ channels. *Neuron.* 27:573–583.

Lecchi, M., E. Redaelli, B. Rosati, G. Gurrola, T. Florio, O. Crociani, G. Curia, R. Cassulini, A. Masi, A. Acrangeli, M. Olivotto, G. Schettini, L. Possani, and E. Wanke. 2002. Isolation of a long-lasting eag-related gene-type K^+ current in MMQ lactotrophs and its accommodating role during slow firing and prolactin release. *J. Neurosci.* 22:3414–3425.

Li-Smerin, Y., and K. Swartz. 1998. Gating modifier toxins reveal a conserved structural motif in voltage-gated Ca^{2+} and K^+ channels. *Proc. Natl. Acad. Sci. USA.* 95:8585–8589.

Li-Smerin, Y., and K. Swartz. 2000. Localization and molecular determinants of the hanatoxin receptors on the voltage-sensing domains of a K^+ channel. *J. Gen. Physiol.* 115:673–684.

Lipkind, G., and H. Fozzard. 1997. A model of scorpion toxin binding to voltage-gated K^+ channels. *J. Mol. Biol.* 158:187–196.

Liu, J., M. Zhang, M. Jiang, and G.-N. Tseng. 2002. Structural and functional role of the extracellular S5-P linker in the HERG potassium channel. *J. Gen. Physiol.* 120:723–737.

MacKinnon, R., and C. Miller. 1989. Mutant potassium channels with altered binding of charybdotoxin, a pore-blocking peptide inhibitor. *Science.* 245:1382–1385.

Miller, C. 1995. The charybdotoxin family of K^+ channel-blocking peptides. *Neuron.* 15:5–10.

Mitcheson, J., J. Chen, and M. Sanguinetti. 2000. Trapping of a methanesulfonanilide by closure of the HERG potassium channel activation gate. *J. Gen. Physiol.* 115:229–239.

Nastainzyk, W., H. Meves, and D. Watt. 2002. A short-chain peptide toxin isolated from *Centruroides sculpturantus* scorpion venom inhibits ether-a-go-go-related gene K^+ channels. *Toxicon.* 40:1053–1058.

Numaguchi, H., F. Mullins, J. Johnson, D. Johns, S. Po, I. Yang, G. Tomaselli, and J. Balser. 2000. Probing the interaction between inactivation gating and d-sotalol block of HERG. *Circ. Res.*87:1012–1018.

Pardo-Lopez, L., M. Zhang, J. Liu, M. Jiang, L. Possani, and G.-N. Tseng. 2002. Mapping the binding site of a HERG-specific peptide toxin (ErgTx) to the channel's outer vestibule. *J. Biol. Chem.* 277:16403–16411.

Park, C.-S., and C. Miller. 1992. Interaction of charybdotoxin with permeant ions inside the pore of a K^+ channel. *Neuron.* 9:307–313.

Ranganathan, R., J. Lewis, and R. MacKinnon. 1996. Spatial localization of the K^+ channel selectivity filter by mutant cycle-based structure analysis. *Neuron.* 16:131–139.

Rauer, H., M. Lanigan, M. Pennington, J. Aiyar, S. Ghanshani, M. Cahalan, R. Norton, and K. Chandy. 2000. Structure-guided transformation of charybdotoxin yields an analog that selectively targets Ca^{2+}-activated over voltage-gated K^+ channels. *J. Biol. Chem.* 275:1201–1208.

Roche, O., G. Trube, J. Zuegge, P. Pflimlin, A. Alanine, and G. Schneider. 2002. A virtual screening method for prediction of the HERG potassium channel liability of compound libraries. *Chem Bio Chem.* 3:455–459.

Roden, D., and J. Balser. 1999. A plethora of mechanisms in the HERG-related long QT syndrome. Genetics meets electrophysiology. *Cardiov Res.* 44:242–246.

Rosati, B., P. Marchetti, O. Crociani, M. Lecchi, R. Lupi, A. Arcangeli, M. Olivotto, and E. Wanke. 2000. Glucose- and arginine-induced insulin

secretion by human pancreatic β-cells: the role of HERG K^+ channels in firing and release. *FASEB J.* 14:2601–2610.

Sanguinetti, M., C. Jiang, M. Curran, and M. Keating. 1995. A mechanistic link between an inherited and an acquired cardiac arrhythmia: HERG encodes the I_{Kr} potassium channel. *Cell.* 81:299–307.

Smith, G., H.-W. Tsui, E. Newell, X. Jiang, X.-P. Zhu, F. Tsui, and L. Schlichter. 2002. Functional up-regulation of HERG K^+ channels in neoplastic hematopoietic cells. *J. Biol. Chem.* 277:18528–18534.

Smith, P., T. Baukrowitz, and G. Yellen. 1996. The inward rectification mechanism of the HERG cardiac potassium channel. *Nature.* 379:833–836.

Spector, P., M. Curran, A. Zou, M. Keating, and M. Sanguinetti. 1996. Fast inactivation causes rectification of the I_{Kr} channel. *J. Gen. Physiol.* 107:611–619.

Stocker, M., and C. Miller. 1994. Electrostatic distance geometry in a K^+ channel vestibule. *Proc. Natl. Acad. Sci. USA.* 91:9509–9513.

Swartz, K., and R. MacKinnon. 1997a. Hanatoxin modifies the gating of a voltage-dependent K^+ channel through multiple binding sites. *Neuron.* 18:665–673.

Swartz, K., and R. MacKinnon. 1997b. Mapping the receptor site for hanatoxin, a gating modifier of voltage-dependent K^+ channels. *Neuron.* 18:675–682.

Torres, A. M., P. Bansal, P. F. Alewood, J. A. Bursill, P. W. Kuchel, and J. I. Vandenburg. 2003. Solution structure of CnErg1 (Ergtoxin), a HERG specific scorpion toxin. *FEBS Lett.* 539:138–142.

Trudeau, M., J. Warmke, B. Ganetzky, and G. Robertson. 1995. HERG, a human inward rectifier in the voltage-gated potassium channel family. *Science.* 269:92–95.

Tseng, G.-N. 2001. I_{Kr}: the hERG channel. *J. Mol. Cell. Cardiol.* 33:835–849.

Tytgat, J., K. Chandy, M. Garcia, G. Gutman, M.-F. Martin-Eauclaire, J. van der Walt, and L. Possani. 1999. A unified nomenclature for short-chain peptides isolated from scorpion venoms: α-KTx molecular subfamilies. *Trends Pharmacol. Sci.* 20:444–447.

Ulens, C., and J. Tytgat. 2000. Redox state dependency of HERGS631C channel pharmacology: relation to C-type inactivation. *FEBS Lett.* 474:111–115.

Wang, K.-W., K. Tai, and S. Goldstein. 1996. MinK residues line a potassium channel pore. *Neuron.* 16:571–577.

Wang, S., M. Morales, S. Liu, H. Strauss, and R. Rasmusson. 1997. Modulation of HERG affinity for E-4031 by $[K^+]_o$ and C-type inactivation. *FEBS Lett.* 417:43–47.

Zhou, W., F. Cayabyab, P. Pennefather, L. Schlichter, and T. DeCoursey. 1998. HERG-like K^+ channels in microglia. *J. Gen. Physiol.* 111:781–794.